Mon. Not. R. Astron. Soc. **330,** 737–754 (2002)

Variable stars in the field of open cluster NGC 6819

R. A. Street,[1★] Keith Horne,[1,2] T. A. Lister,[1] A. Penny,[3] Y. Tsapras,[1] A. Quirrenbach,[4] N. Safizadeh,[4] J. Cooke,[4] D. Mitchell[4] and A. Collier Cameron[1]

[1]*School of Physics and Astronomy, University of St Andrews, North Haugh, St Andrews, Fife KY16 9SS*
[2]*Astronomy Department, University of Texas, Austin, TX 78714, USA*
[3]*Rutherford Appleton Laboratories, Chilton, Didcot, Oxon OX11 0QX*
[4]*Center for Astrophysics and Space Sciences (CASS), University of California, San Diego, CA 92093, USA*

Accepted 2001 November 1. Received 2001 October 4; in original form 2001 June 18

ABSTRACT

We report on the discovery of 25 variable stars plus 13 suspected variables found in the field of the open cluster NGC 6819. The stars were identified from time-series photometric data obtained on the Isaac Newton Telescope, La Palma, during two observing runs covering the 19 nights between 1999 June 22–30 and 1999 July 22–31. The variables found include 12 eclipsing binaries with an additional three suspected, nine BY Draconis systems, plus four variables of other types, including one star believed to be a Cepheid. Three of the 15 eclipsing binaries are believed to be cluster members. Details of a further 10 suspected variable stars are also included.

Key words: binaries: eclipsing – stars: variables: other – open clusters and associations: individual: NGC 6819.

1 INTRODUCTION

Open clusters provide a useful experimental ground for the investigation of star formation and evolution, not least for the variables and in particular, eclipsing binaries that are the subject of work by Kaluzny and others (see for example Kaluzny, Mazur & Krzemiński 1993; Kaluzny & Ruciński 1993; Kaluzny, Krzemiński & Mazur 1996). These and other works suggest that some close cluster binaries evolve considerably with time owing to the gradual loss of angular momentum and eventually coalesce into a single star. Since the ages of clusters can be established independently, the progress of this evolution can be charted by conducting studies such as the current work. As NGC 6819 is an intermediate-age cluster, we might expect to see signs of close/contact binaries in reasonable numbers.

We observed NGC 6819 as part of a search for transits by extrasolar planets. For this project, the wide field of view of the Isaac Newton Telescope (hereafter INT), La Palma, was ideal, allowing us to measure the brightnesses of approximately 30 000 stars in a single exposure. Over two (9- and 10-night) observing runs in 1999 June and July we obtained time-series photometric data on this cluster, and the clusters NGC 6940 and NGC 7789. This data set lends itself naturally to the discovery of variable stars in these fields, and the current work derives from our reduction of the data on the central regions of NGC 6819.

The basic physical parameters of NGC 6819 are provided in Table 1. While this cluster has been well studied in comparison with other clusters, few previous works have obtained long baseline photometry. Nevertheless, some variables have previously been identified in this field: one found by Barkhatova & Vasilevsky (1967) was confirmed by Lindoff (1972), three possible variables were identified by Kaluzny & Shara (1988) and a further possible variable was noted by Manteiga et al. (1991), though these authors commented that the star was too faint to rule out the possibility of large errors causing the variability.

All of the previously identified variables are saturated in our data, so we are unable to provide further information on them. This current work provides long-baseline photometry on this cluster to fainter magnitudes than previously available, and therefore provides a more complete tally of the variables within this field. In Sections 2 and 3 we describe the observations made and the data reduction pipeline developed during the reduction of this first subset of the data. Section 4 presents the photometry of the variables, with finder charts and coordinates supplied for follow-up work, while we summarize the work in Section 5.

2 OBSERVATIONS

We observed NGC 6819 for the 19 nights between 1999 June 22–30 and 1999 July 22–31, on the 2.5-m Isaac Newton Telescope, La Palma, using the Wide Field Camera (WFC). This instrument consists of four 2048×4096 pixel EEV CCDs, covering a $0.28\,\mathrm{deg}^2$ field of view with a pixel scale of $0.33\,\mathrm{arcsec\,pixel}^{-1}$. The gain and readout noise for CCD4 were taken to be $2.22\,\mathrm{e}^-\,\mathrm{ADU}^{-1}$ and $8.4\ \mathrm{e}^-$ respectively from the Cambridge Astronomical Survey Unit webpage.[1] As the hunt for

★E-mail: ras11@st-and.ac.uk

[1] www.ast.cam.ac.uk/~wfcsur/ccd.html

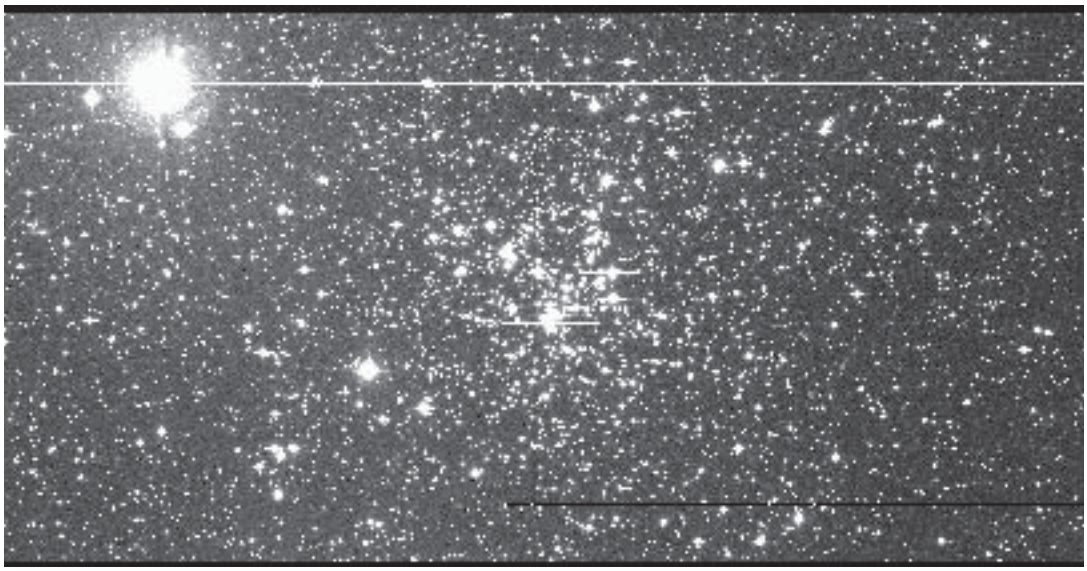

Figure 1. An example frame from the INT data set showing the centre of NGC 6819. North is to the top of the image while east to the left.

Table 1. Basic data on NGC 6819. Data taken from Kalirai et al. (2001) and the SIMBAD and WEBDA data bases.

RA (J2000.0)	$19^{\rm h}41^{\rm m}$
Dec (J2000.0)	$+40°11'$
l	$73\overset{\circ}{.}97$
b	$+8\overset{\circ}{.}48$
Distance (pc)	2500
Radius	$\sim 9.5'$
Age (Gyr)	2.5
Metallicity	+0.07
$E(B-V)$	0.10

exoplanetary transits requires only differential photometry in one colour-band, the observations were made using the Sloan r' filter. The three open clusters NGC 6819, NGC 6940 and NGC 7789 were observed, taking pairs of 300-s exposures of each cluster in turn from the time they became visible. The sequence of exposures was not dithered between frames; we aimed to place each star on the same pixel in each image as far as possible in order to minimize brightness variations owing to pixel sensitivities or stars falling between pixels. In practise, the x, y shifts between images were up to a few pixels. In this way, NGC 6819 was observed for $\sim$7–8 hours each night, typically resulting in 16–25 frames per night, and 325 frames in total over the whole run. The average gap between pairs of exposures of each cluster was, at most, roughly an hour and we had good observing conditions on all nights. The exposure times were tailored to expose the fainter cluster stars optimally for the benefit of transit hunting, which is why many of the stars identified in this cluster by previous authors are saturated in these data. Fig. 1 shows the field covered in this study and illustrates the crowding present particularly in the centre of the cluster.

3 DATA REDUCTION

3.1 PSF-fitting photometry

In order to develop a data-reduction pipeline for this large data set, we have first reduced a subset of the data; the results presented here follow from this reduction. We have concentrated on the Wide Field Camera's central CCD4 frames of NGC 6819.

The debiasing, flat-fielding and trimming of the frames were carried out using the Starlink package FIGARO (Shortridge et al. 1998). A correction for the non-linear response of the chip was also applied, of the form

$$C_{\rm corr} = 0.995565.C_{\rm obs} - 1.10012\times10^{-6}C_{\rm obs}^2 + 5.77076\times10^{-12}C_{\rm obs}^3, \quad (1)$$

where $C_{\rm obs}$ and $C_{\rm corr}$ refer to the number of counts and the corrected number of counts, respectively, for a given pixel after bias subtraction. This correction was taken from the 'Wide Field Camera – Known Problems' webpage.[2] All the frames were collapsed in x and y directions to produce 1D spectra of the frame in each direction. These were then cross-correlated with similar spectra of a selected reference frame in order to determine the relative x, y shifts. Trim limits that would ensure all images were correctly aligned were applied, taking these offsets into account.

The pre-processed frames were then converted into IRAF format using the Starlink package CONVERT (Currie et al. 2000).

The reference frame was reduced using IRAF's DAOPHOT task (Stetson 1987). DAOFIND identified 9541 stars and, after performing aperture photometry, approximately 100 isolated stars were manually chosen for the derivation of the point-spread function (hereafter PSF). The process of selecting PSF stars, generating, refining and subtracting the PSF was iterated until a satisfactory PSF was obtained. Some experimentation was carried out with a number of PSF functions, both fixed-form and position-variable, in order to achieve the best results. It was found that stars subtracted from an image using a fixed PSF showed residuals that varied with position. These residuals were best reduced by employing DAOPHOT's 'penny2' function and allowing it to vary quadratically with position. This is a two component model, consisting of an elliptical Gaussian core and Lorentzian wings. Both parts of the model are aligned along separate and arbitrary position angles. The same PSF stars were used to generate such a

[2] www.ast.cam.ac.uk/~wfcsur/foibles.html

PSF for all subsequent frames. DAOPHOT handles pixel defects, cosmic rays and the like by employing a formula that reduces the weights of pixels that do not converge towards the model as the fit is calculated. This is discussed in more detail in Davis (1994). The post-processing (discussed below) is also able to detect and remove strongly outlying points. Finally, where a star of interest is found to lie close to dead columns/pixels conclusions have been drawn with caution.

In order to apply suitable values of data-dependent variables for each frame, a script was written to produce an IRAF parameter file for each image. These files were then automatically called during the reduction.

Once the parameter files, the full star list and the PSF star list were in place, PSF photometry was performed on the rest of the data set by an automated DAOPHOT script. We chose to have the star positions refitted independently in each frame, having found that the cross-correlation technique aligned the star centroids to around $\sim$1 pixel accuracy.

3.2 Post-processing

The more advanced, position-variable PSF employed during the reduction produced reasonably satisfactory results for most frames. However, for a significant number of images, we found that a position-dependent element still remained in the magnitude residuals, particularly dominant along the long axis of the CCD.

To counteract this problem, and to improve the photometry of the less-affected images, we have developed software to compute position-dependent magnitude zero points for each image in the data set. This was done by splitting each image into 500×500 pixel sectors, and calculating the zero point for each sector in each image independently, using only the stars found within it. Sectors of this size were decided upon after some experimentation as the best balance between considering the variations over small regions of the images and having sectors that incorporated enough stars to calculate meaningful statistics. Ideally, the software would empirically calculate the continuous variation across the image in

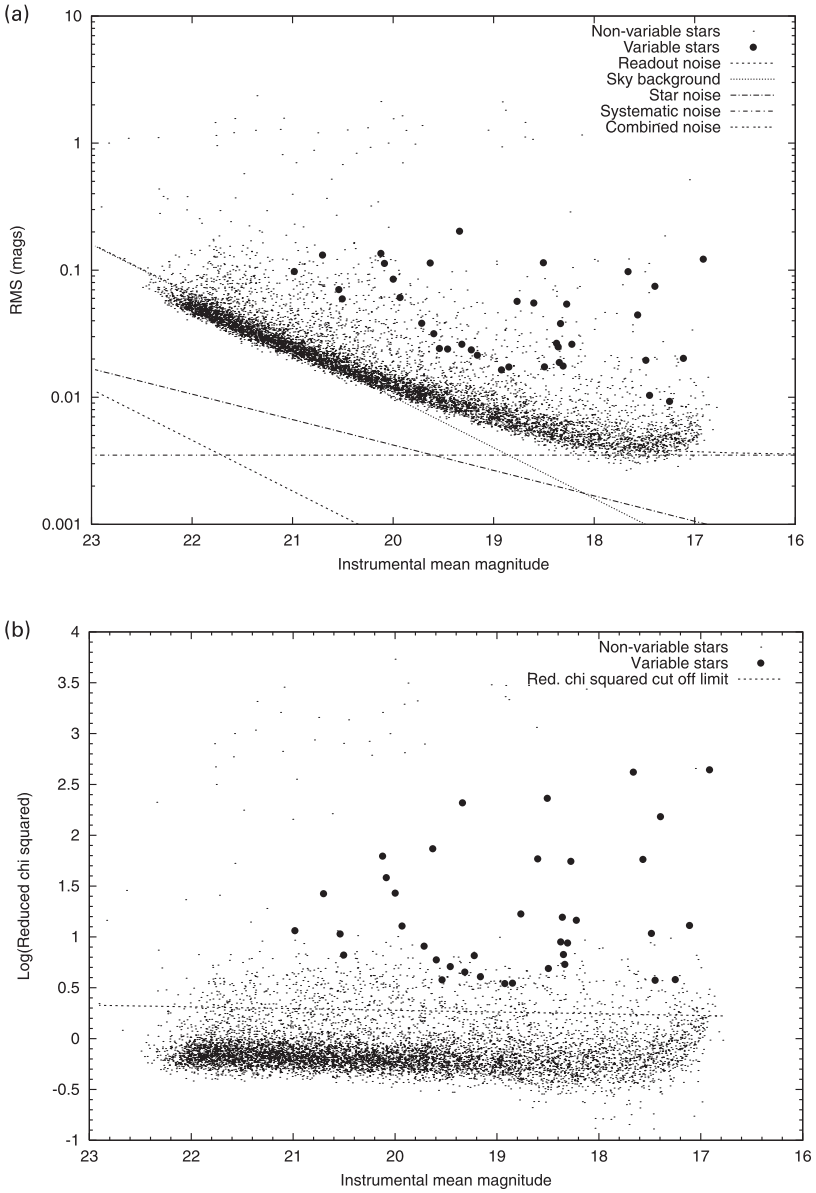

Figure 2. The variation of rms scatter and $\chi^2_{\rm red}$ with instrumental mean magnitude.

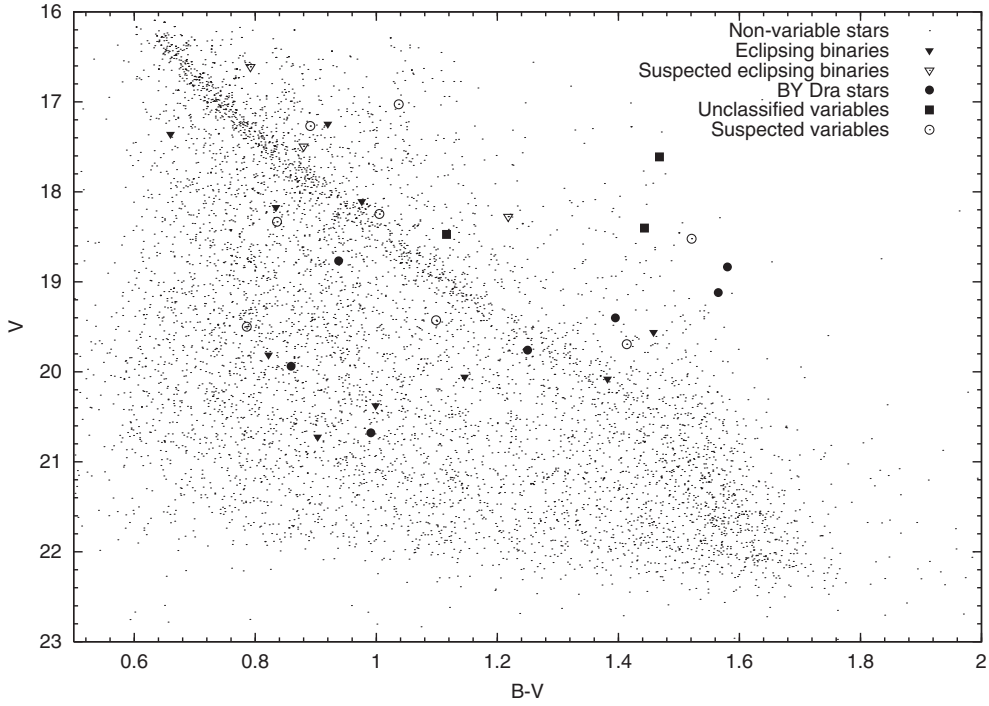

Figure 3. Colour–magnitude diagram of the field of NGC 6819 highlighting the positions of the variables.

two dimensions, and such software is currently under development. It is, however, unnecessary for the detection of the large-amplitude variations highlighted in the current work.

Following this processing, the precision achieved is illustrated by plotting the rms of each star's light curve against its weighted mean magnitude over the whole data set. Fig. 2(a) shows such a plot, and for reference shows the effects of the main expected sources of noise. While some systematic effects remain in the data, our software results in improved precision particularly at brighter magnitudes, where we can achieve the $\sim$0.004 mag precision required to detect planetary transits. We notice that the residual systematic variations are reduced to a level of $\sim$0.0035 mag. After post-processing, these residuals do not appear to show a positional distribution. We also notice that the 'backbone' of points falls slightly below the theoretical noise prediction at the faint end. This is caused by the fact that the theoretical calculations incorporate quantities measured in each image such as sky background etc., and sum the corresponding noise contributions from all images. The rms of each data point, on the other hand, can only include those images in which the star was adequately measured. In a few images, a combination of poor seeing and high sky background contrive to prevent some of the fainter stars from being measured, and so the contribution of this 'noisy' image is removed from the rms of the star.

3.3 Astrometry

Having identified variable stars, astrometry was performed to determine the RA and Dec of each star. A Digital Sky Survey–II (DSS) image covering the field of view was obtained, and a list of star x, y positions was identified from this image using the PISAFIND task within the PISA package (Draper & Eaton 1999). A list of stars covering the whole frame was identified from the Guide Star Catalogue 2.1 (Morrison et al. 2001), and their RAs and Decs were matched with their PISAFIND x, y positions. This list was fed into ASTROM (Wallace 1998), in order to produce more accurate local RA and Dec. positions for all the stars identified in the DSS frame. Around 100 stars common to the DSS and the INT reference frame were then identified, and their x, y positions and RAs and Decs were fed into ASTROM using an eight-parameter solution to calculate RA and Dec positions for all the stars found in the INT reference frame plus the field centre coordinates. The radial distortion coefficient required for this solution was taken from the Cambridge Astronomical Survey Unit webpage.[3] The average rms error in the resulting RA and Dec positions was found to be 0.172 arcsec and 0.180 arcsec respectively.

4 RESULTS

In order to identify variable star candidates, we first needed to eliminate from our sample those stars that were poorly measured. Whatever the reason for this, be it saturation, blending, close presence of a dead column, etc., only stars measured in at least 60 per cent of frames were considered.

The reduced χ^2 of each star relative to the star's mean magnitude was then calculated; these parameters are plotted in Fig. 2(b). We notice that the main body of points on the reduced χ^2 plot are below the expected value of 1. We believe that this is due to the over-estimation of the magnitude errors produced by DAOPHOT, which include default coefficients for the flat-fielding and PSF errors.

A straight line of variable offset and gradient was fitted using the method of least-squares to the 'backbone' of points in this diagram. A good fit was obtained by iteration. The standard deviation of the points around the line ($\sigma_{\chi^2_{\rm red}}$) was computed and, in the following iteration, points more than 2σ away from the line were excluded. This process was repeated until the fitted parameters changed by less than 10^{-5} between iterations. Finally, we identified all stars

[3] www.ast.cam.ac.uk/~mike/casu/WFCsur/distortion.html

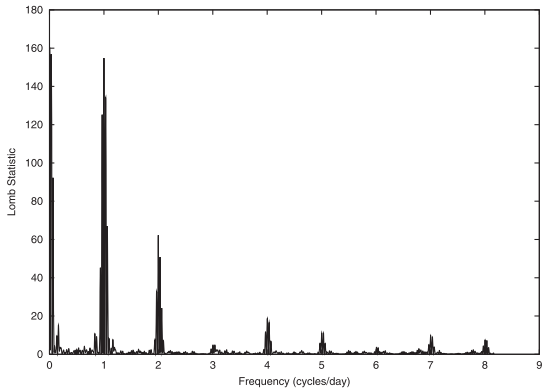

(a) Window Function

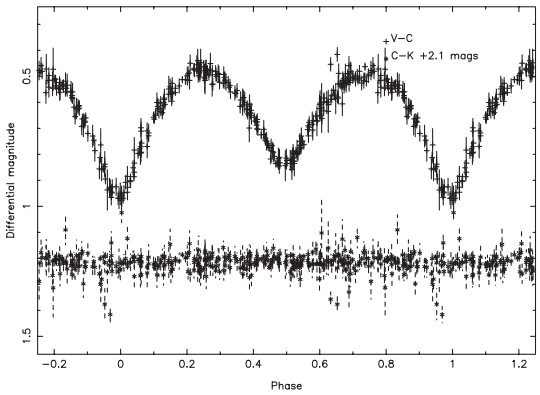

(b) Star 1753

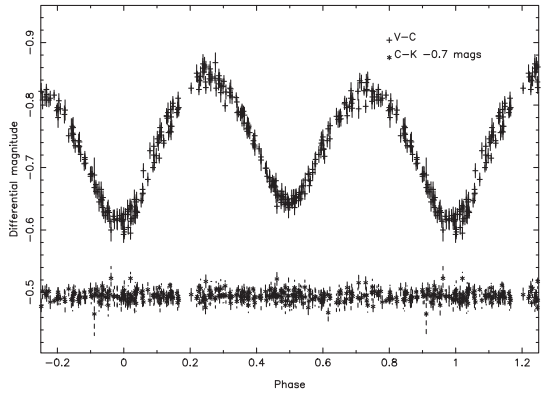

(c) Star 3856

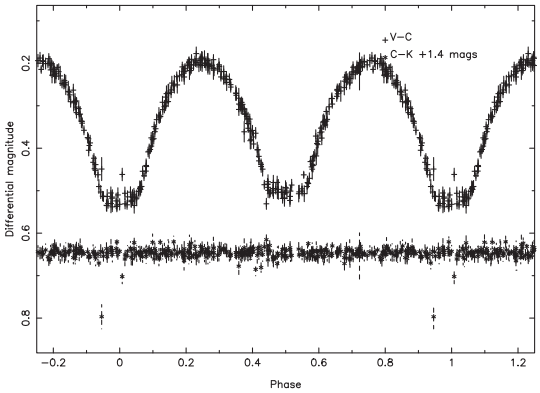

(d) Star 5660

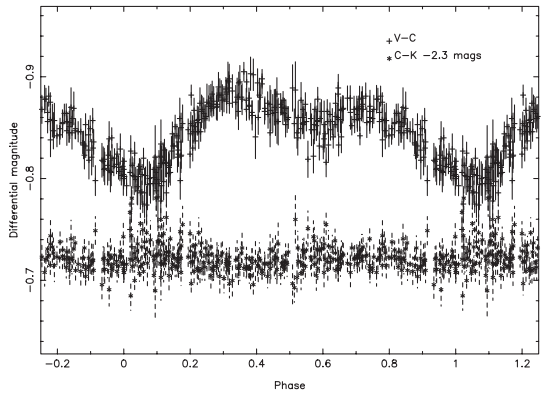

(e) Star 5302

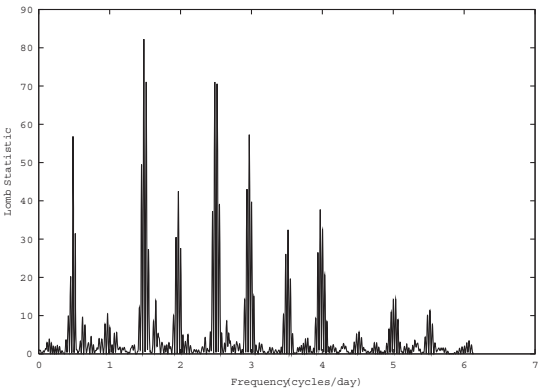

(f) Periodogram of star 5302

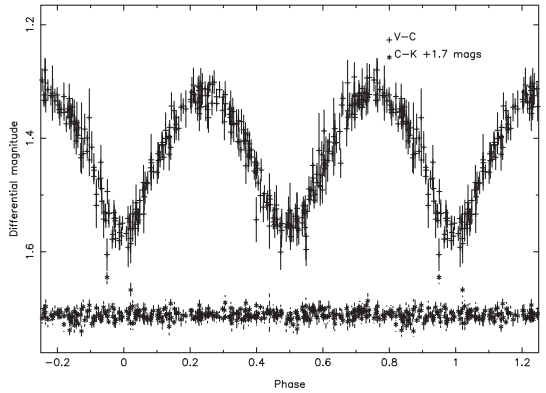

(g) Star 6728

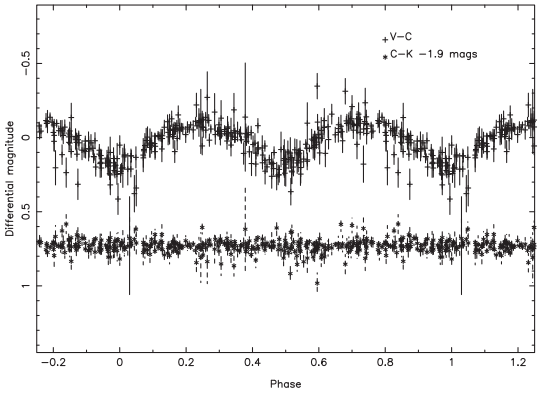

(h) Star 6230

Figure 4. Phased light curves for eclipsing binary systems and the window function for the INT observations.

fulfilling the criterion

$$\chi^2_{\rm red}(j) \geq \chi^2_{\rm red}[\overline{\rm mag(j)}] + \sigma_{\chi^2_{\rm red}}, \quad (2)$$

where $\overline{mag(j)}$, and $\chi^2_{\rm red}(j)$ are respectively the mean magnitude and reduced χ^2 of star j and $\chi^2_{\rm red}[\overline{mag(j)}]$ is the $\chi^2_{\rm red}$ predicted for a star of this magnitude by the fitted lines.

The corresponding cut-off line is plotted in Fig. 2(b). All 785 stars found above this cut-off were considered candidate variables. The light curves of these stars were then examined to eliminate those showing spurious or residual systematic effects. We believe the main reasons for stars showing unusually high scatter are blending, the presence of CCD flaws such as dead columns, and the differences in atmospheric extinction of stars with different colours.

This left us with 25 variable stars plus a further 13 stars showing signs of variability. In these latter cases the photometry is insufficient to be sure (for instance, when the variations are of low amplitude). We attempt to classify these stars below, with the caveat that our lack of spectroscopic data means that the classes should be considered tentative until further work can be carried out. Astrometric results and other data for each star are presented and discussed in the appropriate sections, and finder charts are plotted (in Figs 12–15 later). Light curves of the differential photometry for the stars are also presented in the relevant sections. In order to plot these, comparison and check stars were selected close to each variable; each light curve shows the variable–comparison (V–C) data as the upper curve and the comparison–check (C–K) data as the lower curve. The C–K curves have been displaced in magnitude by the amount shown for the sake of plot clarity.

Visual inspection of the light curves of the 38 stars indicated those that show a high degree of periodicity. A period-finding program was then applied to the data for these stars. This program uses the Lomb method (Lomb 1976) to obtain a frequency spectrum where the highest peak represents the inverse of the period of variability. A Gaussian was then fitted to the highest peak in each spectrum to determine accurately the peak frequency and hence the period. The periodograms of some stars showed more than one strong frequency, indicating more than one possible period. This was usually because the period was close to the 1-d alias, or the result of very short duration eclipses with few data points, or else because the period of the variation was greater than the length of the data set. In these cases, we have phased the light curves on the most likely period, and present the periodogram next to the light curve.

4.1 Colour data and cluster membership

While our current data on this cluster are insufficient to unambiguously determine cluster membership, it is possible to make some distinction between probable members/non-members with the aid of colour information for the stars in our sample.

To this end we were fortunate that Kalirai et al. (2001a) have recently published deep, high-quality multicolour photometry for a very large sample of stars in the field of NGC 6819, which they kindly shared with us (Kalirai, private communication). These data were taken with the CFHT12K mosaic CCD on the Canada–France–Hawaii Telescope, Mauna Kea (hereafter CFHT). For a full description of the observations, reduction and calibration procedures, see Kalirai et al. (2001a,b). Eight of the 12 CFHT12K CCDs overlapped our INT–WFC CCD 4 field.

We have developed our own software in order to identify the stars from our sample in the CFHT results. This software works by computing the following 6-parameter linear transformation between the INT and CFHT coordinates of about eight reasonably bright, isolated stars manually identified in both data sets:

$$X_{\rm CFHT} = X_{\rm INT} + p_1 + p_2 X_{\rm INT} + p_3 Y_{\rm INT},$$
$$Y_{\rm CFHT} = Y_{\rm INT} + p_4 + p_5 X_{\rm INT} + p_6 Y_{\rm INT}. \quad (3)$$

The code then applies this transformation to the stars in our INT sample, and searches through the CFHT data to identify a star at that position. The predicted star positions are typically accurate to less than 1 CFHT pixel (0.206 arcsec pixel^{-1}), although if no star was found within a 4-pixel square box centred on the predicted coordinates, it was assumed that the star was not measured in the CFHT data. Furthermore, stars poorly measured in the INT data, without reliable values of weighted mean magnitude or rms were also not identified in the CFHT colour data. Pixel coordinates were used for this procedure as no World Coordinate System (WCS) or

Table 2. Details of the eclipsing binary systems, classified into the following categories: W Ursae Majoris type (EW), Algol-type (EA) and β Lyrae type (EB). The error on the last decimal place is given in brackets.

Star	RA (J2000.0)	Dec. (J2000.0)	Epoch (HJD)	Period (d)	V mag	$(B-V)$	Type	R′	δm_V (mag)
1753	19 41 52.26	+40 12 23.8	2451358.6315(4)	0.2751(2)	20.078(3)	1.382(8)	EW	6.8	0.15
3856	19 41 28.58	+40 16 24.8	2451356.4608(34)	0.293(1)	17.246(1)	0.920(1)	EW	5.6	0.82
4441[1]	19 41 22.91	+40 14 39.5	2451358.5536(21)	0.2562(8)	18.275(1)	1.218(2)	EW	3.6	1.18
4448[2]	19 41 22.61	+40 11 07.1	2451359.519(2)	0.3032(2)	17.494(1)	0.880(1)	EW	1.0	0.36
5302[3]	19 41 15.27	+40 12 31.8	2451383.326(4)	0.6742(38)	18.106(1)	0.976(2)	EB?	1.3	0.24
5660	19 41 11.73	+40 06 39.7	2451359.6924(8)	0.3384(2)	18.172(1)	0.834(2)	EW	4.7	−0.58
5834[4]	19 41 10.33	+40 15 18.3	2451387.726(1)	0.3660(3)	16.610(2)	0.792(3)	EW	4.2	0.73
6230	19 41 05.84	+40 12 54.3	2451382.4676(8)	0.2814(2)	20.724(4)	0.903(8)	EW?	2.7	−2.75
6728	19 40 59.64	+40 08 25.0	2451359.516(1)	0.2637(9)	19.811(2)	0.822(8)	EW	4.4	−2.29
7333	19 40 53.05	+40 11 17.5	2451385.607(1)	0.3571(2)	20.056(2)	1.146(6)	EA/RS CVn	4.6	−0.92
7916	19 40 44.83	+40 09 23.0	2451391.6151(3)	1.468(2)	17.359(3)	0.660(5)	EA/RS CVn	6.4	−0.92
8080	19 40 42.71	+40 13 25.9	2451355.5551(5)	0.2899(2)	20.374(3)	0.999(7)	EB	6.9	−1.92
8864	19 40 31.55	+40 12 51.8	2451354.569(3)	1.332(3)	20.5(5)		EA	8.8	
8943	19 40 30.48	+40 16 24.1	2451383.567(1)	0.2705(1)	19.559(2)	1.458(5)	EB	10.2	1.06
9440	19 40 21.82	+40 12 08.5	2451355.628(9)	1.451(4)	20.6(5)		EB?	10.5	

[1] Suspected; sits on dead column. [2] Suspected; close to bright star. [3] Crowded field. [4] Suspected; blended, close to dead column.

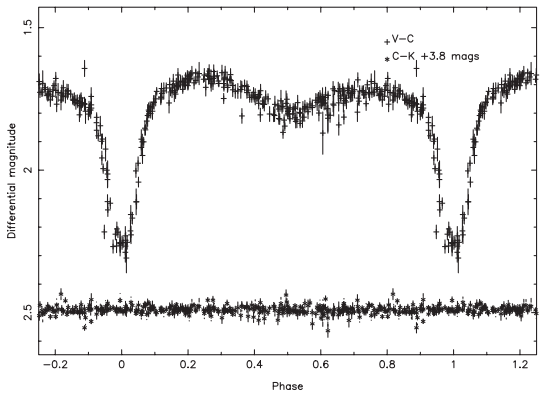

(a) Star 7333

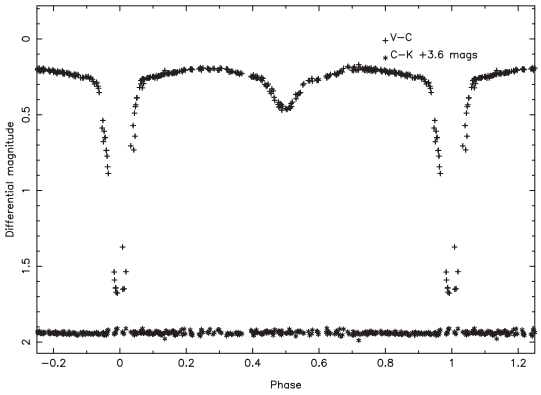

(b) Star 7916

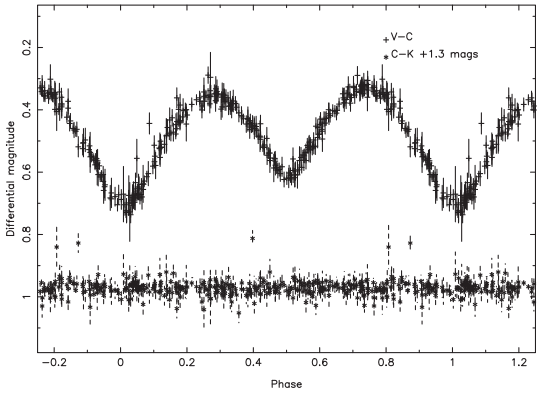

(c) Star 8080

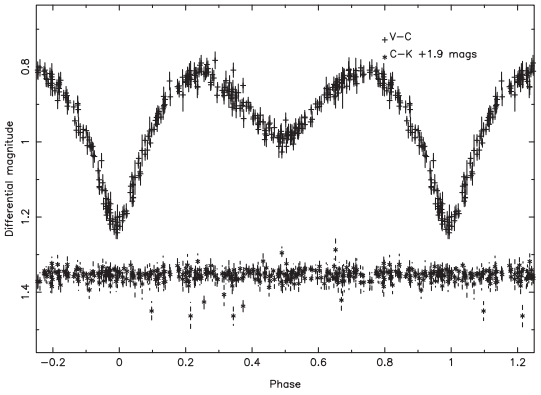

(d) Star 8943

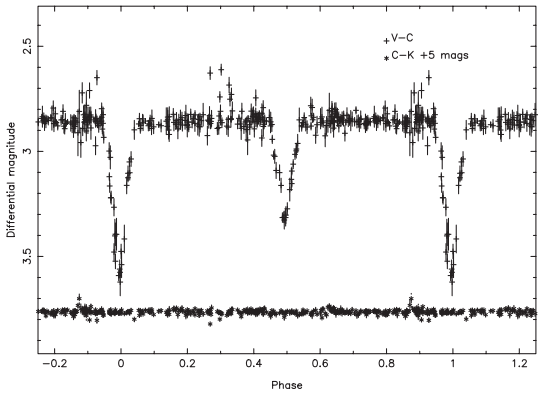

(e) Star 8864

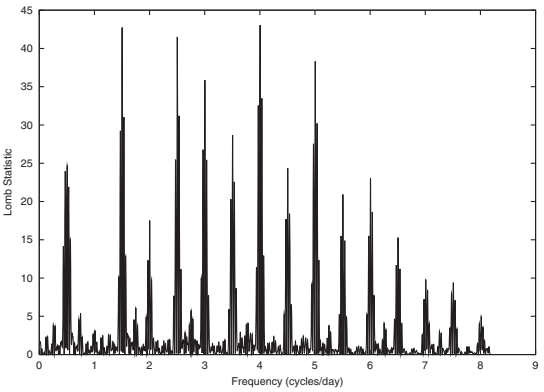

(f) Periodogram of star 8864

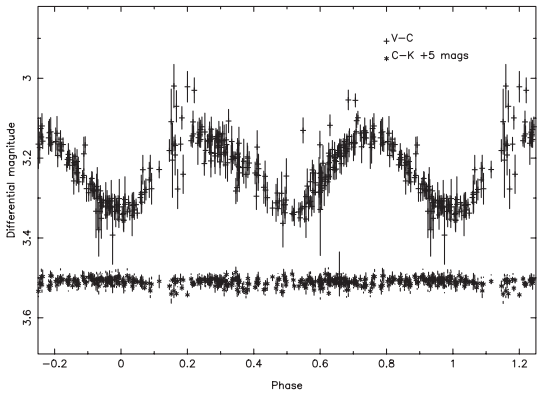

(g) Star 9440

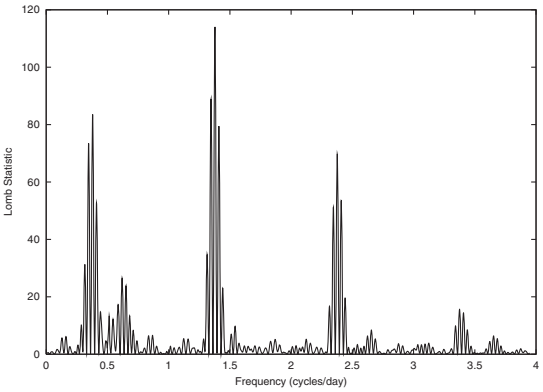

(h) Periodogram of star 9440

Figure 5. Phased light curves for eclipsing binary systems.

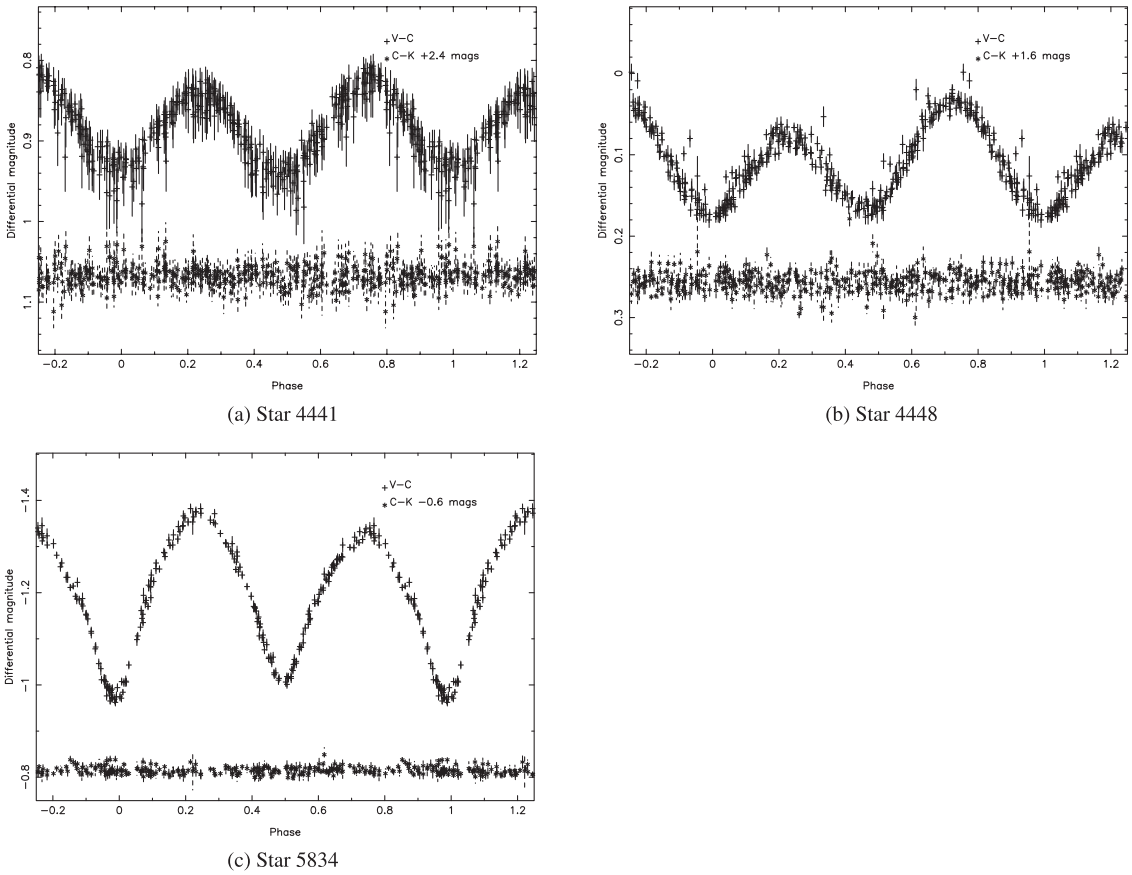

(a) Star 4441

(b) Star 4448

(c) Star 5834

Figure 6. Suspected eclipsing binary systems.

Table 3. Details of BY Dra and unclassified systems. The error on the last decimal place is given in brackets.

Star	RA (J2000.0)	Dec. (J2000.0)	V mag	$(B-V)$	R_I	δm_V (mags)	Type	Amp. (mag)	Epoch (HJD)	Period (d)
224	19 42 11.66	+40 06 48.7	17.611(1)	1.468(2)	11.3	3.07	Unclass	0.02	2451384.323(5)	11.5(20)
1815	19 41 51.38	+40 12 33.6	19.400(2)	1.395(5)	6.6	0.90	BY Dra	0.06	2451388.61(1)	0.733(4)
2393	19 41 44.46	+40 14 23.8	18.765(1)	0.938(3)	6.0	−0.61	BY Dra	0.04	2451356.56(4)	1.9(2)
2576	19 41 41.61	+40 07 03.1	18.833(1)	1.580(4)	6.2	2.49	BY Dra	0.14	2451389.6(3)	1.37(1)
2605[1]	19 41 41.69	+40 11 41.5	18.474(1)	1.116(2)	4.7	0.52	Unclass	0.04	2451389.64(5)	9.6(6)
3126[2]	19 41 36.05	+40 16 19.9	19.939(2)	0.859(5)	6.2	−2.20	BY Dra	0.05	2451384.62(6)	5.4(2)
3127	19 41 35.88	+40 13 53.3	19.758(2)	1.250(6)	4.4	−0.16	BY Dra	0.08	2451386.19(2)	3.5(1)
4003	19 41 26.77	+40 10 49.5	18.2(4)		1.9		BY Dra	0.08	2451384.49(2)	3.9(1)
4484	19 41 22.18	+40 10 11.4	19.1(4)		1.4		BY Dra	0.09	2451357.31(4)	6.3(3)
5861	19 41 09.75	+40 10 38.1	19.120(2)	1.565(4)	1.6	2.11	BY Dra	0.06	2451387.11(5)	6.5(3)
7711	19 40 48.43	+40 16 19.3	20.677(4)	0.991(8)	7.4	−2.26	BY Dra	0.39	2451357.39(3)	4.2(1)
8132	19 40 41.60	+40 07 46.9	19.2(5)		7.6		Cepheid?	0.45	–	–
8830	19 40 32.00	+40 10 40.3	18.402(1)	1.443(3)	8.6	2.14	Unclass	0.15	2451384.61(1)	10.9(8)

[1] Near diffraction spike. [2] Close companion.

astrometry was available. From those stars where colour data was available, we determined the relationship

$$V = 1.0621 r_{\rm INT} - 1.3239 \quad (4)$$

between the INT instrumental magnitudes ($r_{\rm INT}$) and the calibrated V magnitudes from the CFHT. Using this relationship, we were able to provide the roughly calibrated V magnitudes for stars without colour data. These magnitudes are noted in the appropriate tables.

It was also possible to derive a more accurate calibration, using the colour information:

$$V = r_{\rm INT} + 0.4976(B-V) - 0.6504. \quad (5)$$

This was used to ensure that the instrumental magnitude $r_{\rm INT}$ for each star, plus that for its check and comparison stars, was converted to a standardized system before the differential photometry was derived.

This process allowed us to assign calibrated V-band magnitudes and $(B-V)$ values to 6805 stars from our sample, including 31 of the 38 variables (the remaining seven were not measured in the CFHT data set). Fig. 3 presents a colour–magnitude diagram in which the positions of the variables of different types are marked. From this diagram it is clear that many of the variables are not cluster members, but the ∼20 stars positioned above the cluster main sequence could be; further

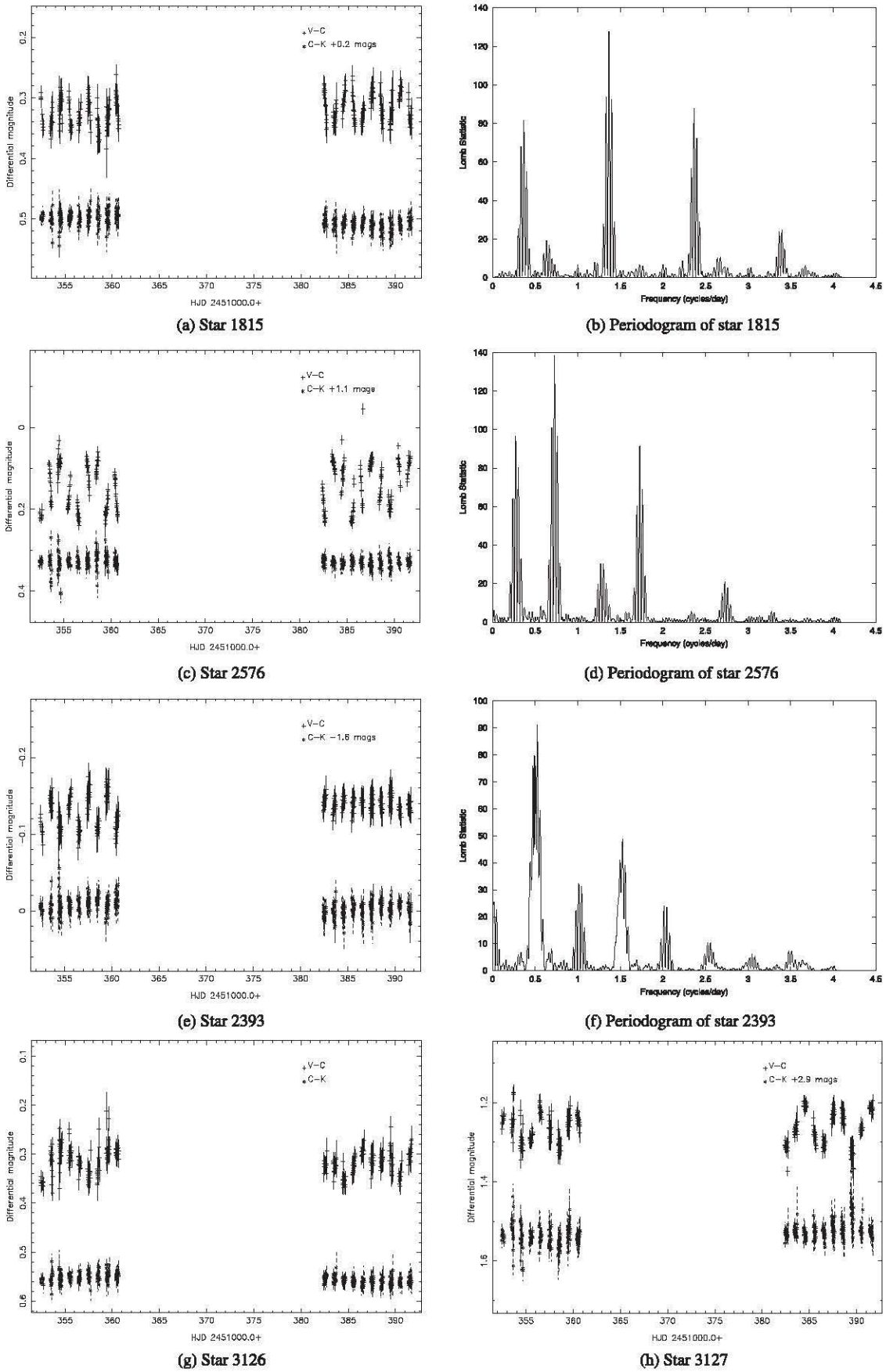

Figure 7. Light curves of the BY Dra systems.

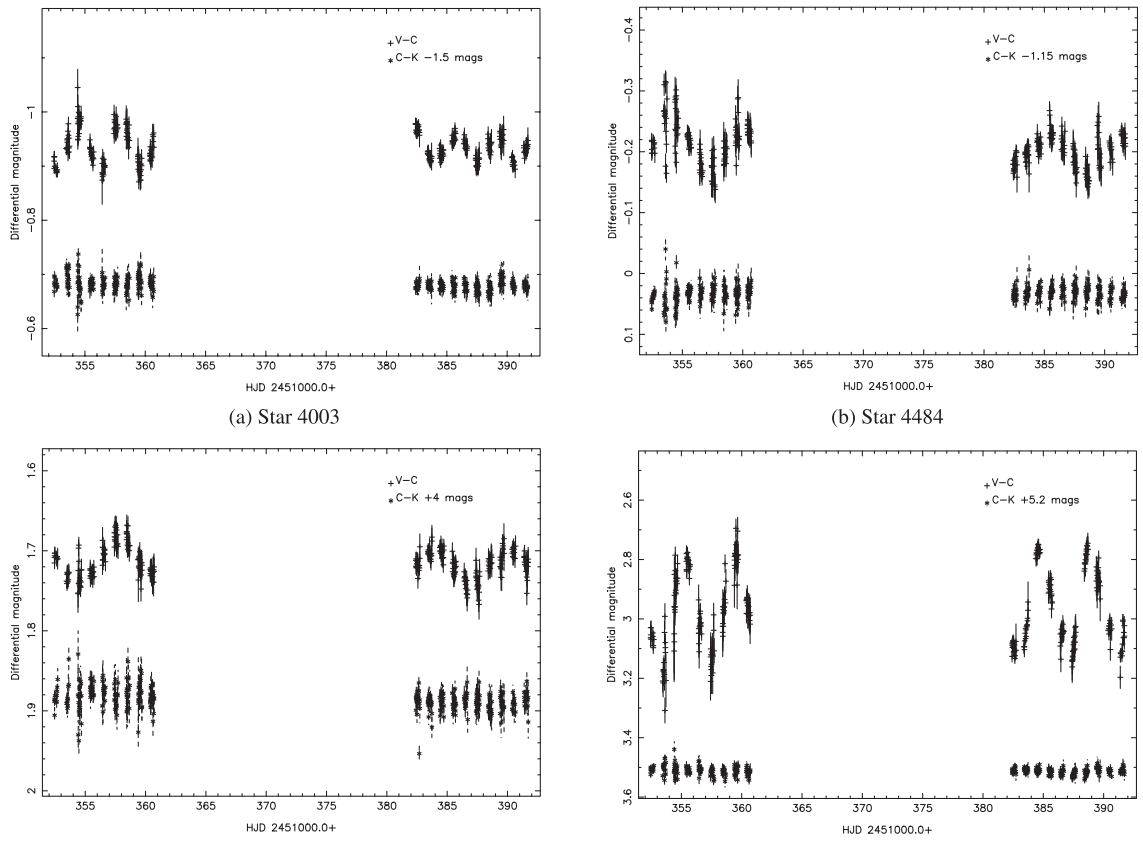

Figure 8. Light curves of the BY Dra systems.

comments for particular stars are made in their relevant section below.

4.2 Eclipsing binaries

We have found 12 eclipsing binary systems, plus a further three systems we suspect to be eclipsing binaries. Their details are listed in Table 2, where in the case of the suspected systems, the reason for caution in our identification is noted. For those stars where colour data and calibrated V magnitudes were available, they are listed in columns 6 and 7 of Table 2; for those stars where none was available we have computed a V magnitude using equation (4). Columns 9 and 10 give the radial distance of each star from the cluster centre [measured by Kalirai et al. (2001a) to be $\alpha_{J2000} = 19^{\rm h}41^{\rm m}17\overset{\rm s}{.}7$, $\delta_{J2000} = +40°11'17''$], and the magnitude difference of each star from the cluster main sequence. In the latter column, a positive value indicates that the star lies above the main sequence, a negative one indicating it lies below the main sequence. These data are intended to be a guide to the likelihood of cluster membership for each star. In particular, the radial distance can be compared with the cluster radius of ∼9.5 arcmin, where the star density falls to that of the field. However, it should be noted that the colours of the binaries were obtained at unknown phase and so the positions of these stars relative to the main sequence is only intended as a rough guide to cluster membership. This is particularly important for some of the larger amplitude binaries.

The phase-folded light curves for these systems are presented in Figs 4 and 5, together with periodograms as required. For comparison, Fig. 4(a) shows the window function of the data set. Those for the suspected systems are shown in Fig. 6. Most of the eclipsing binaries identified are of the W UMa (EW) type, while at least one star seems to be an Algol-type (EA) variable and the remaining four are thought to be detached eclipsing binaries (EB).

Star 5660 stands out as being particularly worthy of further attention. It displays flat-bottomed eclipses of nearly equal depth, suggesting total eclipses, and hence an edge-on orbital inclination. With this in mind, it should be possible to perform a fit to the light curve in order to provide information on mass ratio, temperature etc. The attempt was made using the current data set, but no reliable solution was obtained owing primarily to the lack of time-series data with another filter.

Although the stars 7916 and 7333 were initially classified as Algol-type eclipsing binaries, the distortion in the light curves and inequality of the maxima suggests that they may be eclipsing RS Canum Venaticorum (RS CVn) stars. These binary stars often show similar distortions in their light curves owing to the presence of starspots, but spectroscopy is required to distinguish between these possible types. The photometry for stars 5302 and 9440 is similarly inconclusive about their classifications.

It is interesting to note the distribution in the periods of the W UMa systems. Ruciński (1997) presented a histogram of the period distribution of the W UMa type stars found by the OGLE experiment (Udalski et al. 1995a,b). This indicated that the most frequent period for W UMa systems was around ∼0.4 d, and a sharp period cut-off at ∼0.25 d. While our data suffer from the smallness of the sample, the values in Table 2 suggests that the W UMa systems found in this field have periods shorter than the most common ∼0.4 d period.

On the issue of cluster membership, the data in Table 2 and Fig. 4 indicate that stars 6230, 6728, and 8080 are most likely to be non-members, but is inconclusive about those positioned around the main sequence. Stars 8943 and 9440 are also probably non-members, judging by their large separations from the cluster centre. For the remaining W UMa-type stars in the sample, however, an alternative approach is available thanks to the period–colour–luminosity relation inherent to these stars. Ruciński (1997) derived the following relationship:

$$M_V = -4.44\log(P) + 3.02(B-V)_{\rm o} + 0.12, \qquad (6)$$

where M_V is the absolute magnitude of the W UMa, P is the period and $(B-V)_{\rm o}$ is the dereddened colour of the system. Ruciński (1997) quotes an uncertainty of 0.22 mag on absolute magnitudes calculated from this equation. Supposing that all the W UMa systems in this work that lie above the cluster main sequence are indeed cluster members, we adopt the value of reddening for NGC 6819 derived by Kalirai et al. (2001a), $E(B-V) = 0.10$ mag. We may then calculate the absolute V magnitudes and hence distances of these stars, assuming cluster membership. Our hypothesis of membership holds true for any stars for which the calculated distance matches that of the cluster. In practice, three stars – 3856, 4441 and 5834 – prove to have distances similar to that of the cluster (2500 pc): 2470 ± 252 pc, 2326 ± 237 pc and 2682 ± 275 pc. All of these stars fall slightly above the cluster main sequence on the colour–magnitude diagram, as expected for binary stars.

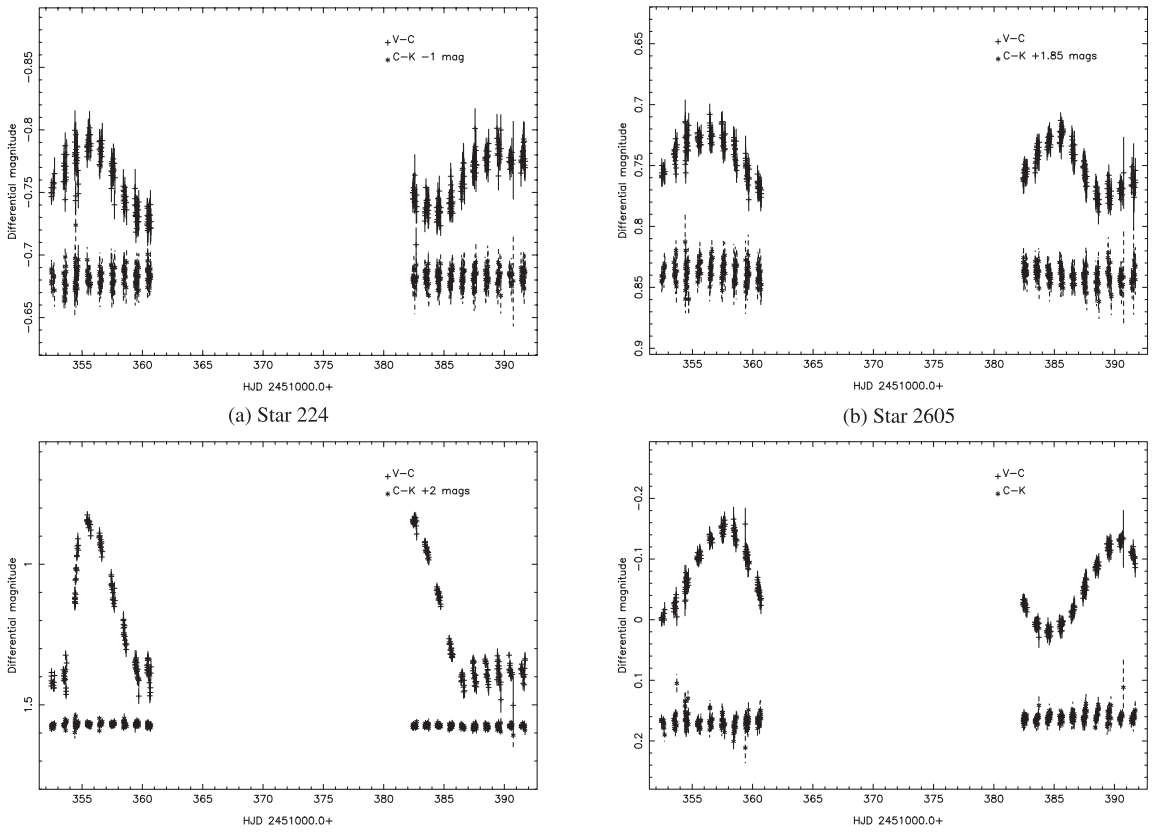

(a) Star 224 (b) Star 2605

(c) Star 8132 (d) Star 8830

Figure 9. Light curves of the unclassified variable stars.

Table 4. Details of suspected variable stars. The error on the last decimal place is given in brackets.

Star	RA (J2000.0)	Dec. (J2000.0)	V mag	$(B-V)$	$R_{\rm I}$	δm_V (mag)
2031	19 41 48.92	+40 14 12.3	18.334(1)	0.836(2)	6.7	−0.73
2501	19 41 42.74	+40 08 40.2	19.427(2)	1.099(4)	5.5	−0.51
2825	19 41 39.15	+40 13 26.8	19.693(2)	1.414(6)	4.7	0.70
3236	19 41 34.26	+40 06 34.9	17.027(1)	1.037(1)	5.6	1.61
3878	19 41 28.16	+40 12 32.9	17.269(1)	0.891(1)	2.4	0.64
4339	19 41 23.67	+40 11 52.2	17.0(4)		1.4	
5371	19 41 14.72	+40 12 14.2	18.247(1)	1.005(2)	1.1	0.24
5590	19 41 12.60	+40 12 06.5	18.7(4)		1.2	
8152	19 40 41.72	+40 13 37.7	19.499(2)	0.786(3)	7.1	−2.19
8741	19 40 33.50	+40 15 57.6	18.520(1)	1.521(3)	9.5	2.45

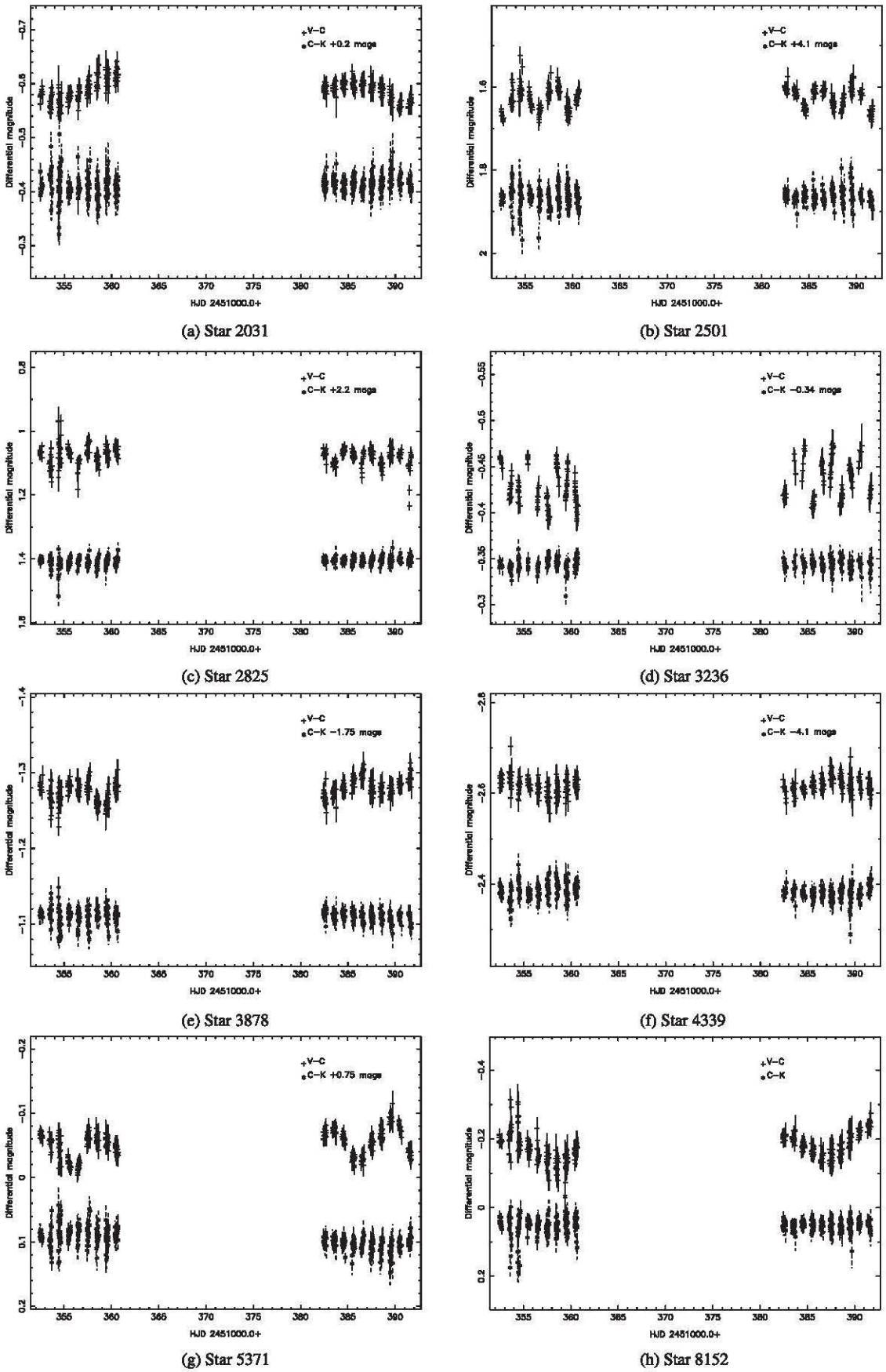

Figure 10. Light curves of the suspected variable stars.

4.2.1 Star 8864

Star 8864 also deserves special attention. The shape of this star's light curve seems to indicate a detached system of two spherical stars, and yet the period was found to be 1.332 d. It must be pointed out that the periodogram of this data, shown in Fig. 5(f), has a number of strong peaks and therefore potential periods. This structure is believed to be caused by the scarcity of data points obtained during the brief eclipses. All of the periods highlighted by the strong peaks have been used to phase the data for this star: only the peak at ∼1.5 produced a phased light curve and not scattered data points. The period implied is a harmonic of this peak. For two stars to remain undistorted at what must be a fairly small separation implies that both stars are of low mass and radius. Although no colour information is available for this system, its mean out-of-eclipse magnitude of 20.5 mag, and the likelihood that it consists of two small, low-mass stars, suggests that the system is relatively nearby and not a cluster member (this is supported by its wide separation from the cluster centre). The duration and depth of the eclipses, ∼5 h and 0.75 mag, 0.45 mag respectively, tend to argue for main-sequence star-sized components. It is possible to derive a range of possible component masses for this system, using Kepler's law written in the form

$$P = \frac{0.116(a/\mathrm{R}_\odot)^{3/2}}{(M/\mathrm{M}_\odot)^{1/2}}, \qquad (7)$$

where P is the period of the system in days, a is the orbital separation, M is the sum of the component masses and $\mathrm{R}_\odot$, $\mathrm{M}_\odot$ are the solar radius and mass respectively. By rearranging equation (7) it is possible to calculate the orbital separation of the stars for various component masses. Furthermore, knowing that the stars are undistorted implies that they must have radii $R_* \lesssim 0.1a$ (Hilditch 2001). It is therefore possible to estimate the maximum undistorted radius for components of various spectral types. The estimated maximum radius can then be compared with the radius of a star of the type used. If the radius of the spectral type concerned is greater than the maximum calculated, then it implies that stars of that type are too large to remain undistorted given the period of this system. In this way, we find that star 8864 most probably consists of a pair of late-M dwarfs. Very few such systems are currently known, so further study of this system is recommended.

4.3 BY Draconis stars

We have found nine stars which appear to be of the BY Draconis (BY Dra) type; their details are tabulated in Table 3, and their light curves are presented in Figs 7 and 8. While periods have been determined for these stars, in some cases the periods are a sizeable fraction of the length of the data set. Therefore, as few cycles were observed the periods show a higher degree of uncertainty. Columns 6 and 7 of Table 3 refer to radius from the cluster centre and magnitude difference from the main sequence, as described in Section 4.2. Most of these stars show the classic characteristics of BY Dra stars – sinusoidal photometric variations (given in column 9 of Table 3) attributed to starspot activity on time-scales of a few

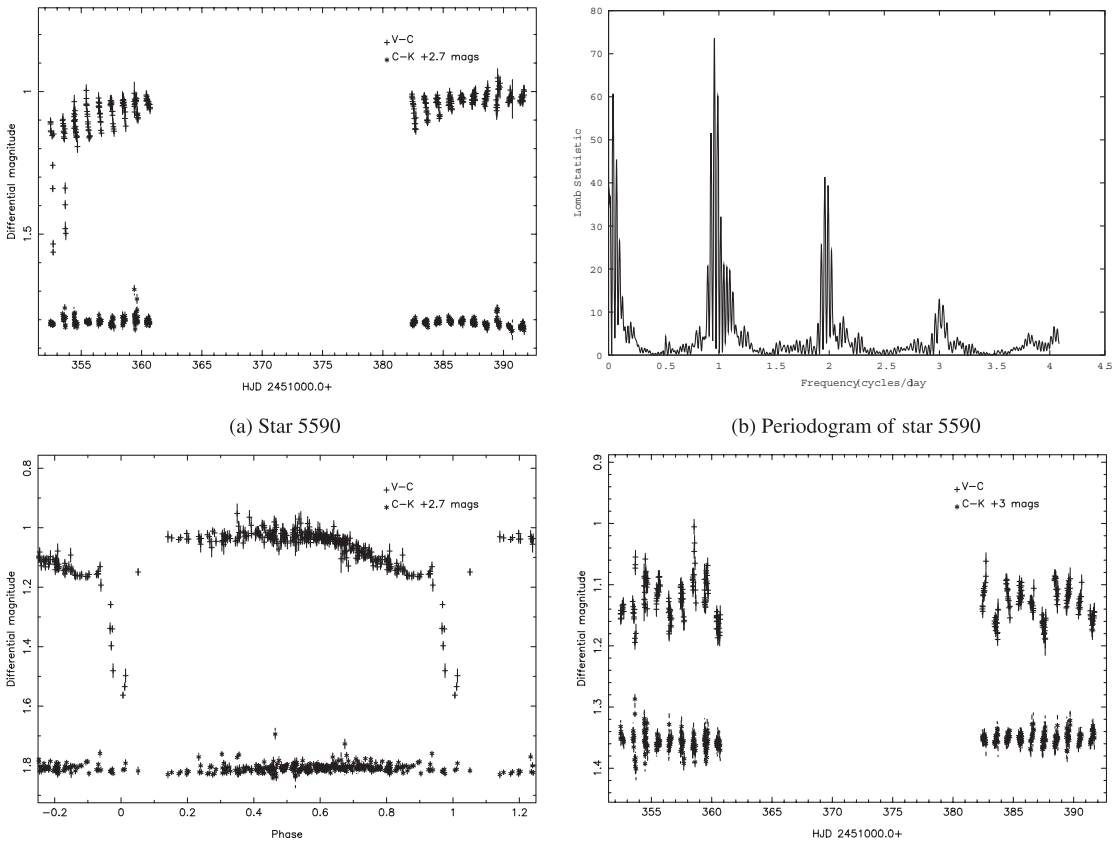

(a) Star 5590

(b) Periodogram of star 5590

(c) Phased lightcurve of star 5590

(d) Star 8741

Figure 11. Light curves of the suspected variable stars.

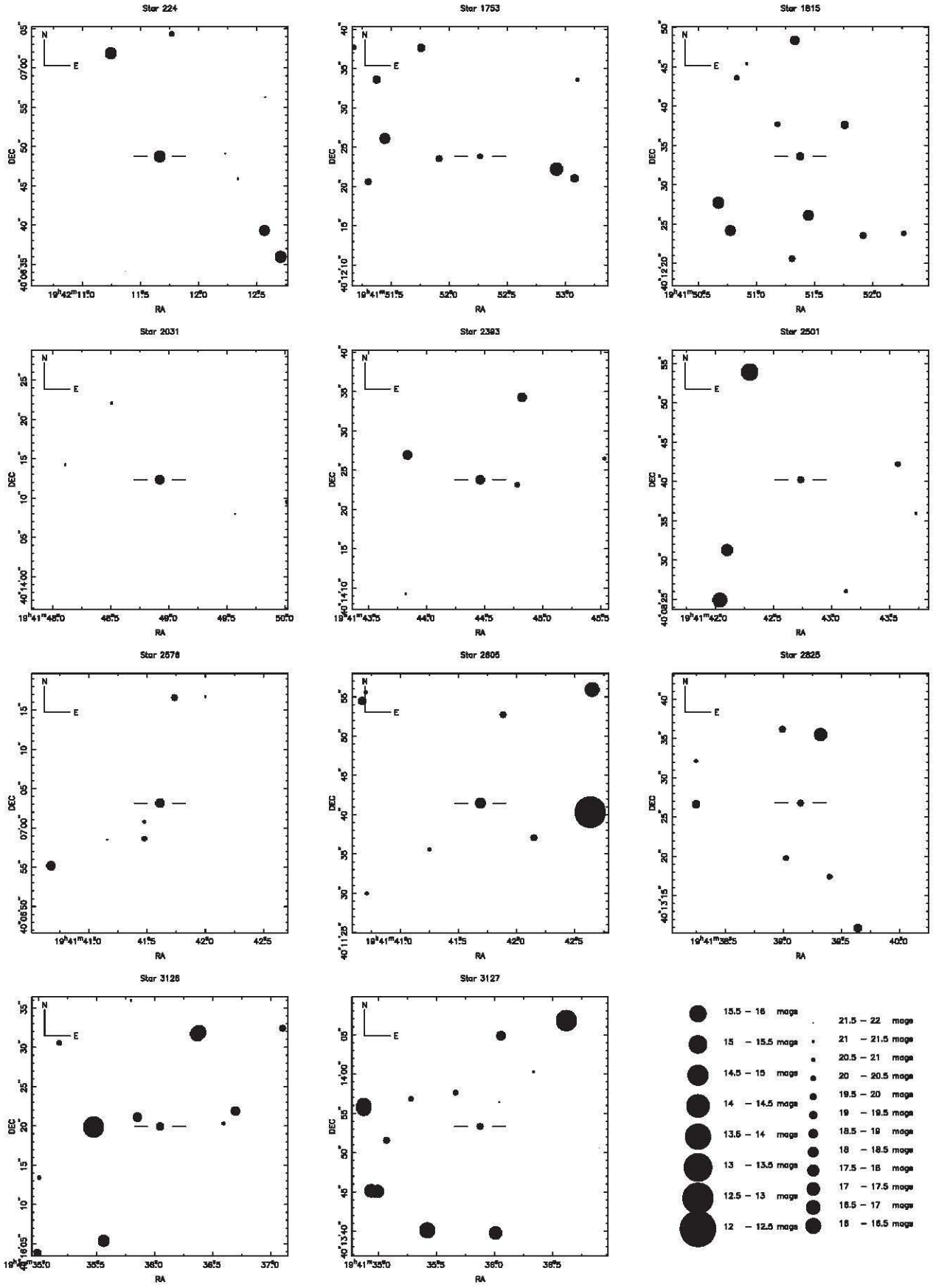

Figure 12. Finder charts for the variable stars in numerical order.

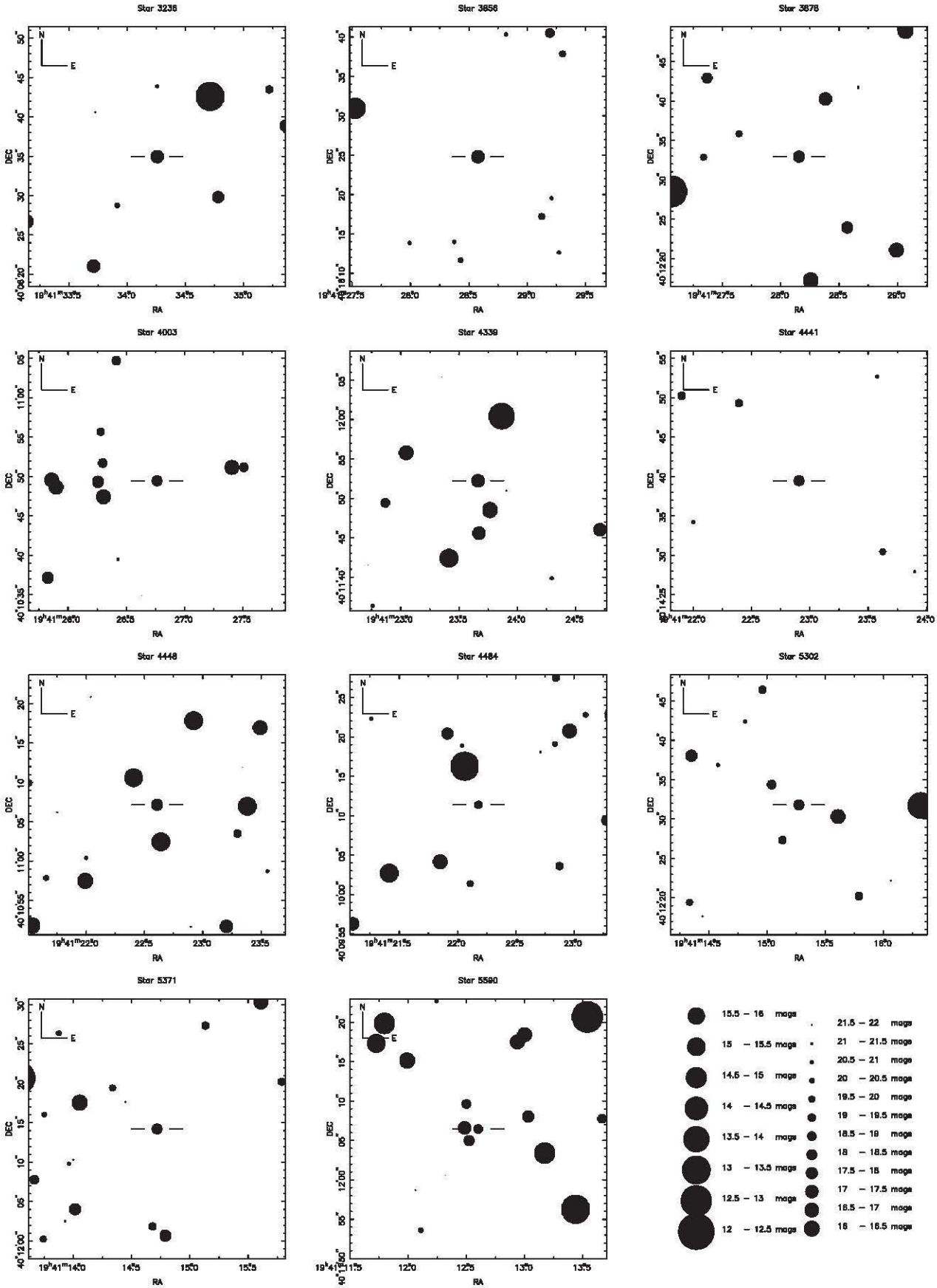

Figure 13. Finder charts for the variable stars in numerical order.

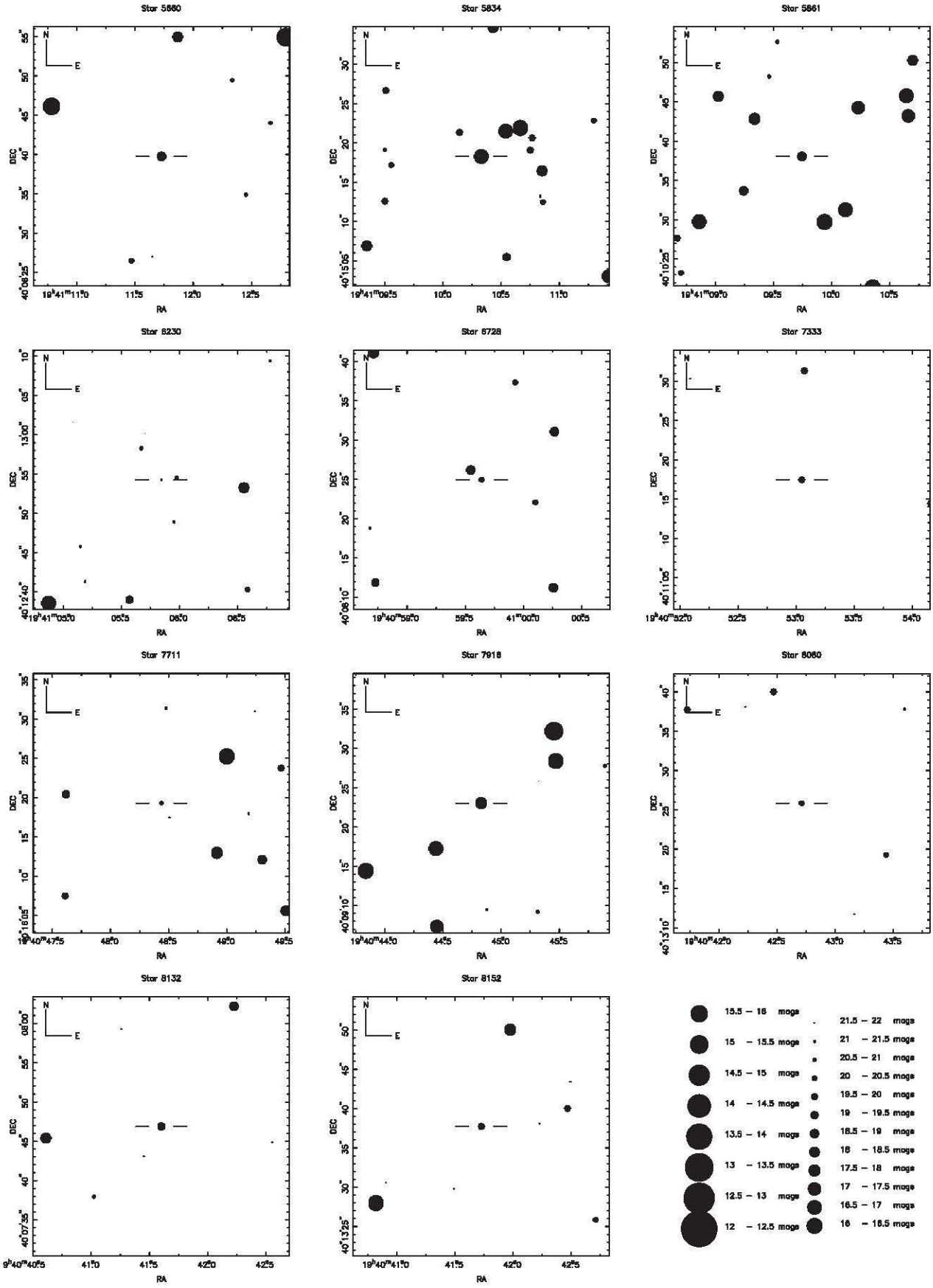

Figure 14. Finder charts for the variable stars in numerical order.

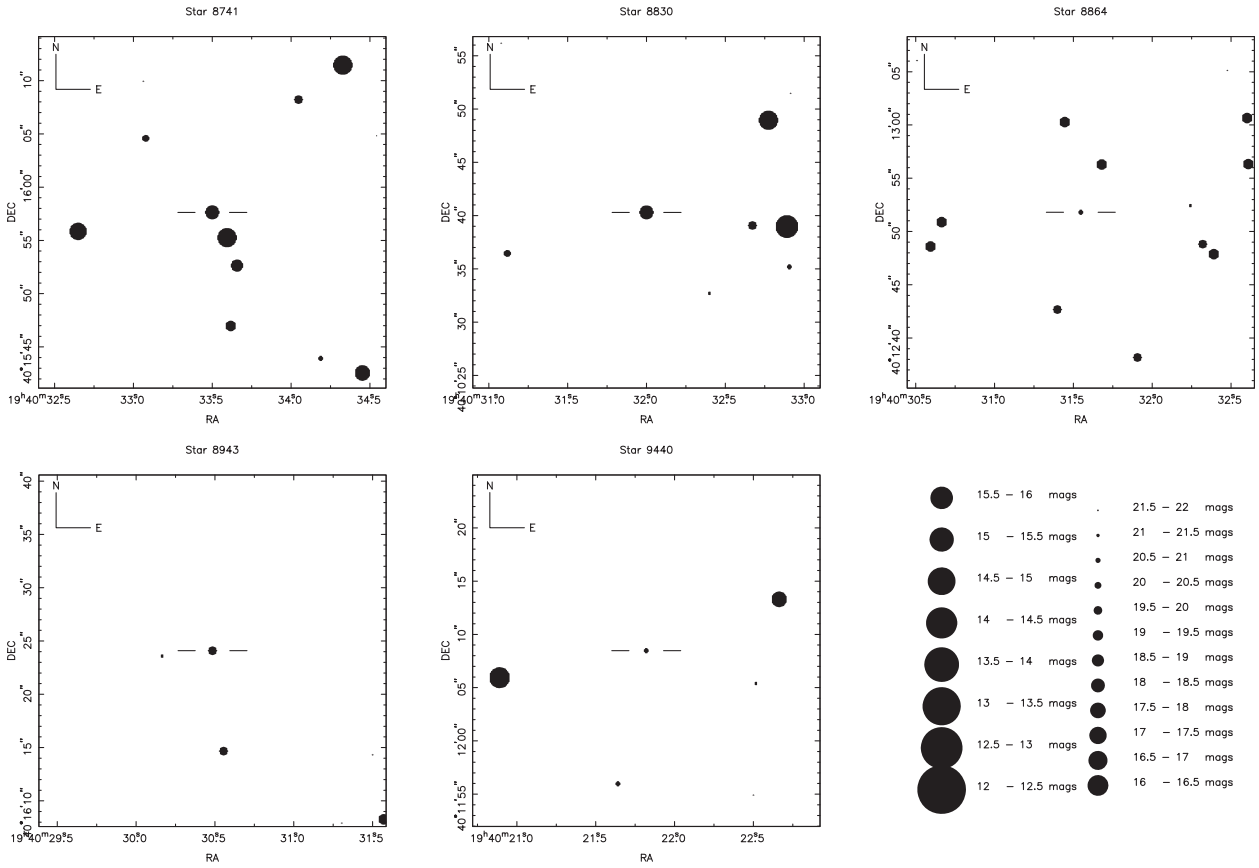

Figure 15. Finder charts for the variable stars in numerical order.

to tens of days, with photometric amplitudes between 0.05 and 0.5 mag. Alekseev (2000) found that the majority (80 per cent) of BY Dra stars do not exceed an amplitude of 0.15 mag, and our data conform to this finding. Only one star, 7711, displays an unusually high amplitude of nearly 0.4 mag. However, this is similar to the amplitude of BY Dra itself (0.38 mag, Alekseev 2000), and other examples of ∼0.4 mag amplitude BY Dra stars are known, so we retain this classification for 7711, in lieu of further data on this star. Furthermore, the $(B - V)$ colour information available for these objects indicate late-type stars, which is consistent with our classification. Some of these stars show a change in the amplitude of the variations between the two data sets, most notably 2393. This makes sense in terms of the constantly changing area of spot coverage of the stars.

Fig. 4 highlights 1815, 2576, 3127 and 5861 as possible cluster members, and while we have no colour information for 4003 and 4484, both have small projected distances from the cluster centre. The remaining stars are unlikely to be cluster members.

The stars 1815, 2576 and 2393 are notable exceptions from the norm with a considerably shorter period of $\lesssim 2$ d. If further work confirms our classification, it may be that these stars have been spun up as part of binary systems, or they may simply be younger objects and unrelated to the cluster. We note, however, that the period of 2393 in particular is such that we obtained similar phase observations each night, and the resulting gaps in our phase coverage precludes firm classification.

We note that RS Canum Venaticorum (RS CVn) and FK Comae Berenices (FK Com) stars can show similar light-curve morphology to BY Dra stars, if the binary is non-eclipsing in the case of an RS CVn. While the high frequency of binary stars would argue for at least some of the stars in this section being RS CVn stars, we have currently have no evidence for this being the case. The possibility of a FK Com classification can be ruled out for most of our candidate BY Dra stars on the basis of their colours which indicate late-type stars. However, it remains a possible classification for the two stars (4003 and 4484) with no $B - V$ information. Until spectroscopic data is available for these objects, we classify them as BY Dra stars.

4.4 The unclassified and suspected variables

We found four other stars showing significant variability for which the classification remains tentative. The details of these stars are given in Table 3, and their various light curves may be found in Fig. 9.

The light curve of star 8132 (Fig. 9c) appears to be that of a Cepheid. While we have no colour data to indicate cluster membership for this star, if our classification is correct, then it is a pulsating giant star of high luminosity (class Ib–II) and spectral type F–K, according to Kholopov et al. (1985). Gray (1992) quotes the absolute V-magnitude of F5–K5 Ib giants to be -4.6 to -4.5 mag. At its faintest, therefore, and including the effects of extinction [$E(B - V) = 0.10$, Kalirai et al. 2001a], a Cepheid member of NGC 6819 would have an apparent magnitude of ∼8 mag. For comparison, the brightest stars present in our field of observations have magnitudes reaching ∼16 mag, and stars brighter than these were completely saturated in all our exposures.

If further observations prove that star 8132 is a Cepheid, it is certainly not a cluster member.

The other three unclassified stars remain enigmatic, owing to the long period and low amplitude of their variation. We consider that they are most likely to be early-type contact binaries with low orbital inclination or possibly ellipsoidal variables. The colour data for all three place them above the main sequence and so the question of membership remains open, but the large projected separations of 224 and 8830 suggest that they are not cluster members.

Table 4 lists the details of stars we suspect may be variable but where the photometry is not sufficient to confirm this, owing to low-amplitude variations or poor measurements resulting from faintness, blending, etc. Their light curves are presented in Figs 10 and 11. Owing to the nature of the photometry, we have not attempted to classify these stars, but five of the candidates (2825, 3236, 3878 and 5371) could be cluster members from their colour data and projected separations, and we recommend their further study.

Star 5590 is particularly worthy of interest. This object has been classified as a suspected variable owing to the unusual nature of its variations combined with the position of the star in the densest part of the cluster where blending is considerable. Nevertheless, with this caveat in mind, the data appear to justify its inclusion. As Fig. 11(b) illustrates, the variability appears to be periodic. Fig. 11(c) shows the light curve phased on this period. The light curve is incomplete because this period is so close to one day: 1.04 ± 0.10 d. These plots seem to indicate an eclipsing binary system, possibly consisting of a small object such as a white dwarf (indicated by the short primary eclipses) and a large, cool body (the lack of secondary eclipse indicates that most of the light is contributed by the primary). The curious dip shortly before the primary eclipse could be the eclipse of a 'hot spot' on the secondary star caused by the heating of the primary. However, this is by no means certain; if this periodicity proves correct, extended study will be necessary to acquire complete data on this object. The finder charts for all these variables are presented in Figs 12–15.

5 CONCLUSIONS

We present long-baseline Sloan r' photometry for over 9500 stars in the field of the intermediate-age open cluster NGC 6819. We find evidence for 25 variable stars within this sample plus a further 13 where variability is suspected. Of these 38 stars, 12 are thought to be eclipsing binaries with an additional three suspected, nine are BY Draconis systems, and four remain unclassified owing to long-period variation, though one of these is believed to be a Cepheid. However, we urge caution regarding these classifications until confirmation is possible via spectroscopy and/or further photometric observations. We have determined that three of the W UMa-type eclipsing binaries are likely to be cluster members from their $(B - V)$ colours and periods, and have ruled out membership for at least 12 variables of other types, including the Cepheid, should the classification prove correct.

These results support the work of Kaluzny and others, which suggest that W UMa systems form in significant numbers in open clusters of around 4–5 Gyr (see Kaluzny et al. 1993, 1996; Kaluzny & Ruciński 1993). We can see that such systems, which form from initially detached binaries, are just beginning to appear in cluster NGC 6819, which is only ~2.5 Gyr old. Following up this work with spectroscopic and further photometric observations would be valuable, as cluster variables can potentially reveal much about stellar formation and evolution in this environment, and many basic details remain to be confirmed, such as our initial classifications and membership indications.

ACKNOWLEDGMENTS

We extend our thanks to Jasonjot Kalirai for kindly agreeing to share his CFHT results with us prior to their public release. RAS would also like to thank Ron Hilditch and David James for many helpful discussions. This research made use of the SIMBAD data base operated at CDS, Strasbourg, France and the WEBDA data base operated at the University of Lausanne, Switzerland. RAS was funded by a PPARC research studentship during the course of this work. The data reduction and analysis was carried out at the St Andrews node of the PPARC Starlink project. This paper is based on observations made with the Isaac Newton Telescope operated on the island of La Palma by the Isaac Newton Group in the Spanish Observatorio del Roque de los Muchachos of the Instituto de Astrofisica de Canarias.

REFERENCES

Alekseev I. Y., 2000, SvA, 77, 784
Barkhatova K. A., Vasilevsky A. V., 1967, Var. Star Bull., 16, 171
Currie M. J., Privett G. J., Chipperfield A. J., Berry D. S., 2000, Starlink User Note 55.12, Rutherford Appleton Laboratory
Davis L. E., 1994, A Reference Guide To The IRAF/DAOPHOT Package. NOAO, Tucson AZ
Draper P., Eaton N., 1999, Starlink User Note 109.10, Rutherford Appleton Laboratory
Gray D. F., 1992, The observation and analysis of stellar photospheres. 2nd edn. Cambridge Univ. Press, Cambridge
Hilditch R. W., 2001, An Introduction to Close Binary Stars. Cambridge Univ. Press, Cambridge
Kalirai J. S. et al., 2001a, AJ, 122, 257
Kalirai J. S. et al., 2001b, AJ, 122, 266
Kaluzny J., Ruciński S. M., 1993, MNRAS, 265, 34
Kaluzny J., Shara M. M., 1988, AJ, 95, 785
Kaluzny J., Mazur B., Krzemiński W., 1993, MNRAS, 262, 49
Kaluzny J., Krzemiński W., Mazur B., 1996, A&AS, 118, 303
Kholopov P. N. et al., 1985, General Catalogue of Variable Stars. 4th edn. Nauka, Moscow
Lindoff U., 1972, A&AS, 7, 497
Lomb N. R., 1976, Ap&SS, 39, 447
Manteiga M., Martinez Roger C., Morales C., Sabau L., 1991, A&A, 251, 49
Morrison J. E., Röser S., McLean B., Bucciarelli B., Lasker B., 2001, AJ, 121, 1752
Ruciński S. M., 1997, AJ, 113, 407
Shortridge K., Meyerdierks H., Currie M. J., Clayton M., Lockley J., Charles A., Davenhall C., Taylor M., 1998, Starlink User Note 86.16, Rutherford Appleton Laboratory
Stetson P. B., 1987, PASP, 99, 191
Udalski A., Olech A., Szymanski M., Kaluzny J., Kubiak M., Mateo M., Krzeminski W., 1995a, Acta Astron., 45, 433
Udalski A., Szymanski M., Kaluzny J., Kubiak M., Mateo M., Krzeminski W., 1995b, Acta Astron., 45, 1
Wallace P. T., 1998, Starlink User Note 5.17, Rutherford Appleton Laboratory

This paper has been typeset from a TEX/LATEX file prepared by the author.